

Military Technical College
Kobry El-Kobbah
Cairo, Egypt



10th International Conference
On Aerospace Sciences &
Aviation Technology

AN ASSESSMENT TO THE DESIGN OF TAIL BOOM STRAKES BY CFD-TECHNIQUES

Ahmed A. Saad*

Single-rotor helicopters are exposed to asymmetric flow over the tail boom that causes an aerodynamic force in the sideward direction. Unfortunately, this side force is in an opposite direction to the tail rotor thrust and hence reduces the pedal margin. This problem could be overcome by a proper design of spoiler/strake on the suction side of the tail boom. Design of tail boom strakes is commonly done via intensive wind tunnel testing. In this paper, the author introduces an assessment to a less-costly and more-convenient alternative based upon one of the commercial CFD software in the market. A tail boom model of circular cross-section that was previously tested in the subsonic wind tunnel facility at NASA Langley has been adopted for this purpose. The Navier-Stokes equations with $k-\varepsilon$ turbulent model are solved over unstructured grid of triangular elements. The computational and experimental measurements of the force coefficients for the model without strakes were found in good agreement for a wide range of flow incidences. For the model with two strakes, this agreement was found limited to only a range of incidences of $\pm 20^\circ$.

KEY WORDS

Aerodynamics, Computational Fluid Dynamics

*Ph D in Aerospace, Egyptian Air Force.

NOMENCLATURE

C_x	Side force coefficient, $C_x = \frac{\text{Side force per unit length}}{2 R_1 q}$
C_y	Normal force coefficient, $C_y = \frac{\text{Normal force per unit length}}{2 R_1 q}$
q	Dynamic pressure, $q = 0.5 \rho V^2$ [N/m ²].
R_1	Radius of the circular section [m].
R_2	Radius of the outer boundary [m].
Re	Reynolds number, $Re = \rho V (2R_1) / \mu$.
R_{mr}	Radius of main rotor [m].
V	Main rotor down wash speed at the tail boom section [m/s].
x	Lateral coordinate [m].
y	Vertical coordinate [m].
μ	Coefficient of dynamic viscosity [kg/m sec].
ρ	Free-stream air density [Kg/m ³].
ϕ	Angle of flow incidence [deg], +ve clockwise.

Abbreviations:

CFD	Computational Fluid Dynamics.
R&D	Research & Development.
NASA	National Aeronautics and Space Administration.

INTRODUCTION

Single-rotor helicopters experience asymmetric airflow over the tail boom in hover and low-speed flight that results in significant side aerodynamic loading. This phenomenon is the result of the spiral-flow nature of the main rotor wake during hovering, the tail rotor wake, and the crosswind velocity component (See Fig.1). The outcome is a side force component that works in a direction opposes the tail rotor thrust. So a portion of the tail rotor power is wasted in overcoming the adverse side force. Besides, the motion of the point of separation on the tail boom suction side causes variations in the pressure field on this side that eventually leads to lateral oscillation of the tail boom. The solution to this problem has been devised through a proper design of a tail boom strakes. The strakes are L-shaped metal plates that work as spoilers and installed on the suction side of the tail boom. The purpose is to create a large area of turbulent flow on the suction side and hence builds up the pressure on this side (See Fig 2). Moreover, the presence of strake fixes the separation point of the flow over the suction side and hence eliminates the lateral fluctuations of the tail boom. By a proper design of tail boom strakes, large portion of the power consumed by tail rotor to overcome the tail boom sideward aerodynamic loads can be saved. The saved power can be used in improving other performance characteristics such as: pedal margin, payload, rate of climb, cross wind speed limitations, and fuel consumption.

A wind tunnel investigation [1] was conducted at the NASA Langley 4x7- Meter subsonic wind tunnel on three tail boom sections represents the AH-64 (Apache), UH-60 (Black Hawk), and UH-1H (Bell). The cross section was taken at station approximately 80% of the main rotor radius (R_{mr}), where the maximum rotor wake velocities are

generally experienced in hover (See Fig. 3). Two-dimensional aerodynamic forces and pressure distributions were obtained for a flow incidence ranges from -45° to 90° and dynamic pressure range from 1.5 to 50 psf. The effects of pro-turbulences such as tail rotor drive-shaft covers and spoilers were investigated. Of the tail boom shapes tested, the circular cross section without the drive-shaft cover had the least aerodynamic side force. Addition of shaft cover to each shape changed side and vertical forces significantly. The addition of spoilers at selected locations shifted the side force in a favorable direction over a wide range of flow angles. Consequently, there is a potential for reducing the amount of directional control required in hover and sideward flight through a reduction in tail rotor thrust required. Although the spoiler increases down load, the net effect is an improvement in helicopter performance. Later on, another investigation has been conducted [2] at the same facility focusing on cross sections represents the OH-58A and OH-58D helicopters. The aerodynamic forces were measured for flow incidence ranges from -45° to 90° and dynamic pressure from 5 to 15 psf. The results indicate a significant improvement at conditions, which represent right sideward flight by reducing the adverse aerodynamic side force with strakes installed. These data were used to calculate a change in tail rotor power for the full-scale helicopter and indicated approximately 5% to 6% savings in right sideward flight for the critical velocity range 0-30 Knots. The results indicated a potential for reducing the directional control effort in hover and sideward flight with an increase in the main rotor power required due to the increase in boom vertical loading. The overall net improvement in power is about 0.5% for both the OH-58A and OH-58D.

In this paper, the CFD approach to the problem of tail boom strake design is assessed. A cross-section represents a circular conical tail boom such as those of the (MI-8, MI-17,) helicopters was chosen for this study to simplify geometry. CFD analysis was conducted for test conditions similar to that in [2] using the *ANSYS FLOTRAN* software [3]. The full Navier-Stokes equations with $k-\varepsilon$ turbulent model are solved over unstructured grid of triangular elements with proper refining at the cylinder surface and strake area. Side and vertical force measurements were conducted for the model with and without strakes. Results were analyzed and compared with that obtained in the NASA Langley subsonic wind tunnel. Computational results for the case of strakes uninstalled were found in good agreement with the experimental data for a wide range of flow incidences. For the case of strakes installed, the computational results were found in good agreement only for the range of incidences from -20° to 20° . Flow field velocity observations were utilized to determine the best strake location.

MODEL GEOMETRY AND CFD ARRANGEMENT

The model is for a circular cross-section [2] that represents a conical tail boom with two strakes mounted on one side (see Fig.4). The outer boundary is circular with radius five times the model radius to ensure undisturbed flow conditions at the outer boundary. A two-dimensional unstructured grid of triangular elements was adopted to mesh the model with appropriate refining on the cylinder surface, especially at the area of strakes connection with the boom (see Fig.5). The *FLOTRAN* module of the *ANSYS* software [3] was utilized to model the viscous flow over the boom. The unsteady Navier-Stokes equations were employed with a $k-\varepsilon$ turbulent model that has inlet turbulence intensity of .01 as stated in [2].

RESULTS AND ANALYSIS

The first set of computations was done for the model without strakes at the flow conditions stated in Table.1. The results were presented in terms of the course of variation of side (Fig.6) and vertical (Fig.7) force coefficients with flow incidence angles. The results depicted in Fig.6 and Fig.7 demonstrates good agreement with the experimental data for a wide range of flow incidences (up to 50°).

The second set of computations concerned with the model with two strakes mounted on the left side of the model with the arrangement stated in Table.2. The CFD model was able to resolve the flow physics over the two strakes as demonstrated by the velocity contours (Fig.8) and the vector plots of the velocity field (Fig.9). Also, the particles flow traces (Fig.10) for $\phi=20^\circ$ resolves the vortex scheme created by the two strakes. In spite of the physical consistency of the CFD model, the variation of the side force (Fig.11) and vertical force (Fig.12) coefficients show good agreement only in the range $|\phi|<20^\circ$, especially for the vertical force coefficient. In general, it was observed that the CFD estimation for the side force coefficient is always a little bit higher than the corresponding wind tunnel measurements for the model with/without strakes (Fig.6 & Fig.11 respectively). On the other hand, the vertical force coefficient computations were always a little bit lower than its corresponding wind tunnel measurements for the model with/without strakes (Fig.7 & Fig.12 respectively). The limited agreement of force measurements to small incidences is - of course - related to the inadequate simulation of the computational model to capture the complex flow phenomena at high incidences. The disagreement of force measurements is also related partially to the numerical errors encountered in the computational algorithm of force measurements, especially for

surfaces with sharp corners (as the strakes). In another way, if the experimental pressure distributions were available it might be in better agreement than the force measurements. The benefits gained by the strake are shown in Fig. 13 through the large increase in side force coefficient in the positive direction that saves the tail rotor power. However, a part of the saved tail rotor power is lost by the increase in vertical force coefficient as demonstrated in Fig. 14.

CONCLUSIONS

Recently, commercial CFD software has been widely spread with the availability of PC-versions for the majority of applications. In this study, the utilization of commercial CFD software in tail boom strakes design is assessed, which can provide quick and cheap prediction especially in the preliminary design phases. The study concluded that the computational approach to the design of strakes for a conical tail boom has provided force measurements with very good agreement for the case without strake. For the case with two strakes the flow dynamics gets more complicated, which was reflected on the force measurements. The inadequacy of the force measurement computational algorithms over surfaces with sharp corners is also contributing to the disagreement of force measurements. The CFD model was able to capture the complex flow dynamics but the agreement of force measurements was marginal ($\phi \in [-20^\circ 20^\circ]$).

REFERENCES

- [1] Wilson, J. and Kelley, H., "Aerodynamic Characteristics of Several Current Helicopter Tail Boom Cross Sections Including the Effect of Spoilers" NASA-TP-2506, (1986).
 - [2] Crowell, C. and Kelley, H., "Aerodynamic Effect of Strakes on Two-Dimensional Tail Boom Models of OH-58A and OH-58D Helicopters" NASA-TM-4248, December (1990).
 - [3] ANSYS Inc., "ANSYS 5.4 Software, the FLOTRAN Module" ANSYS Inc., (1997).
-

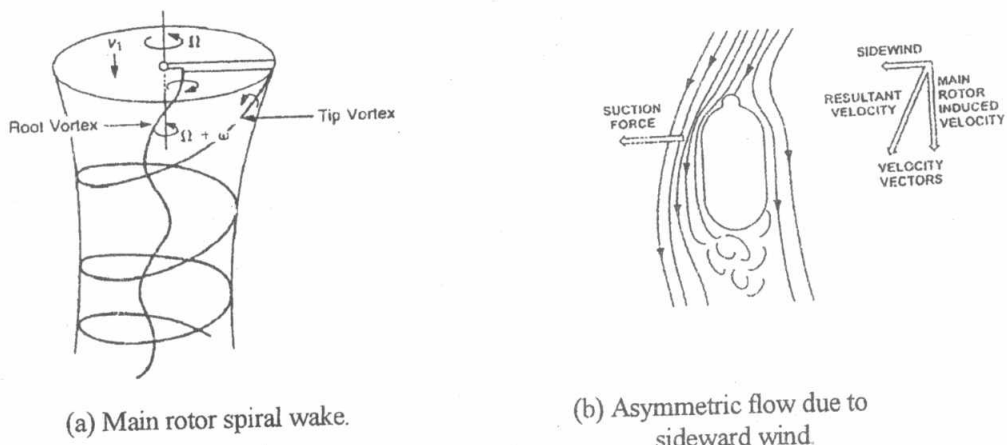


Fig.1 Asymmetric flow on tail boom cross section

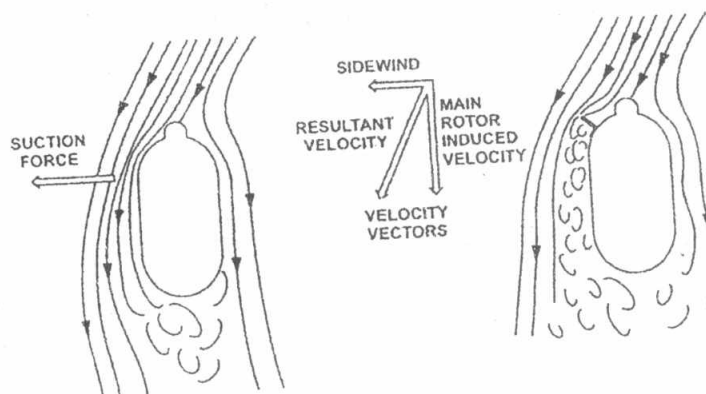


Fig.2 Strake pro-turbulent effect

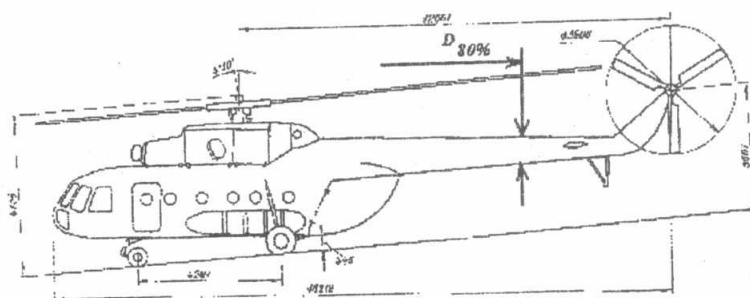


Fig.3 Tail boom station of the cross section model

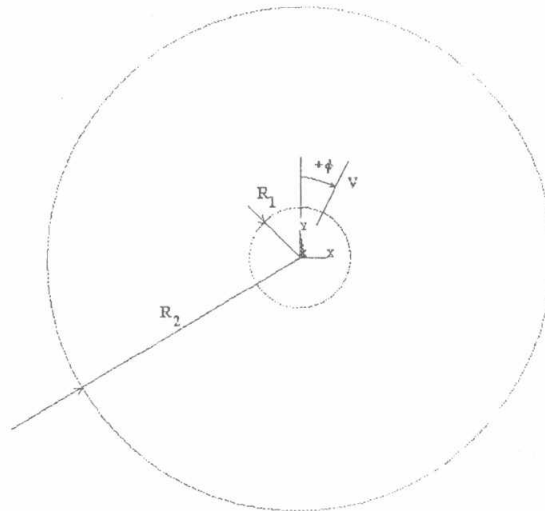
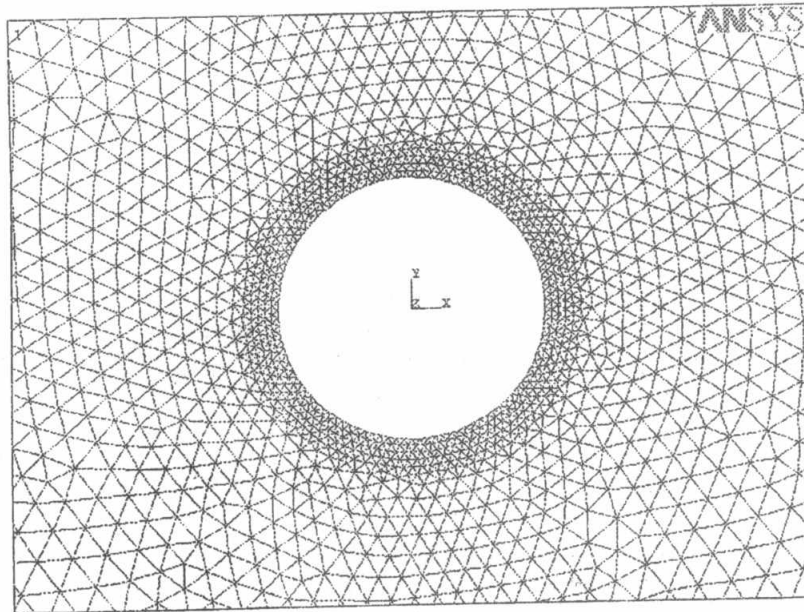


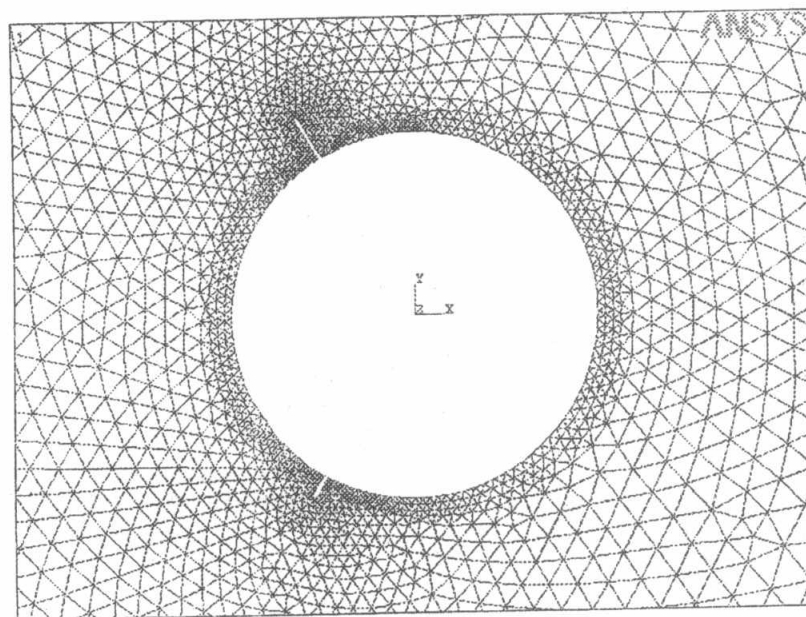
Fig.4 Model geometry and sign conventions

Table.1 Model parameters

Parameter	Value
Model Radius (R_1) [m]	0.19
Radius of Outer Boundary (R_2) [m]	0.95
Dynamic Pressure (q) [psf]	15
Reynolds Number (Re)	0.87×10^6



(A) With strake uninstalled



(B) With strakes installed

Fig.5 Unstructured grid of triangular elements for the model with/without strakes

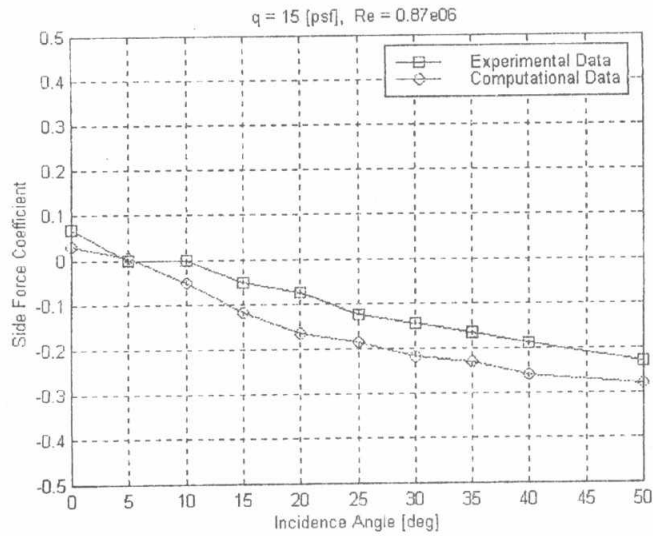


Fig. 6 Variation of the side force coefficient with flow incidences of the circular section without strakes for the NASA wind tunnel measurements [2] and Computational results

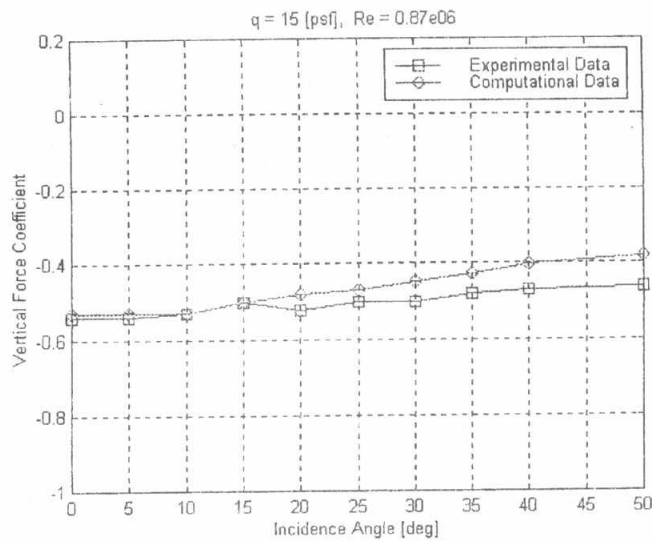


Fig. 7 Variation of the vertical force coefficient with flow incidences of the circular section without strakes for the NASA wind tunnel measurements [2] and Computational results

Table.2 Strakes configuration

Strake Number	Height [cm]	Thickness [mm]	Angular Position [deg]
1	5	6	-30°
2	2.5	6	-150°

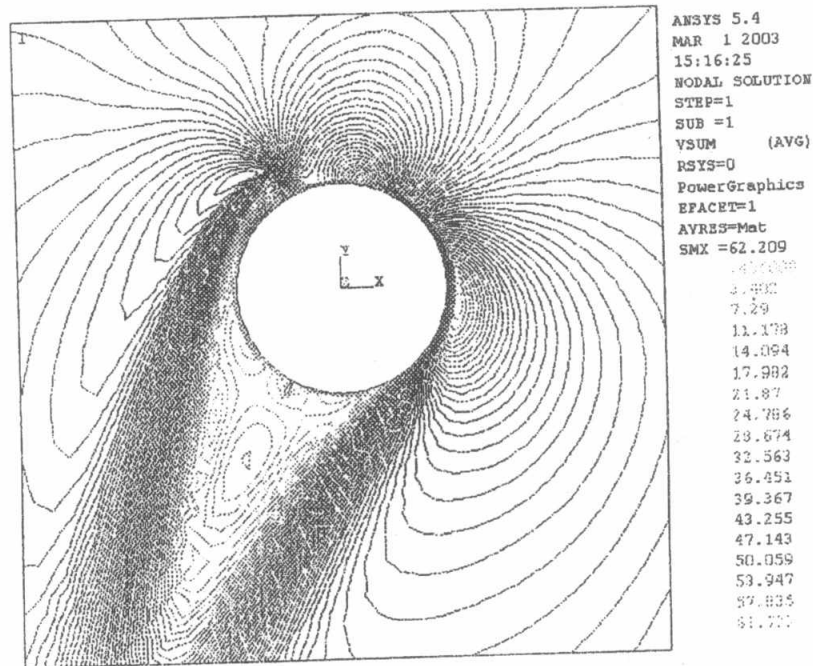


Fig.8 Velocity contours for the model with 2 strakes for the flow at 20° incidence

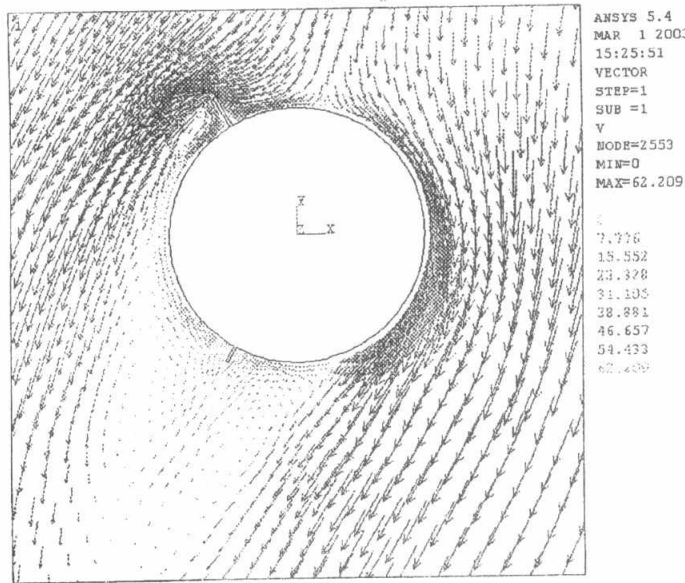


Fig.9 Vector plotting for the velocity field for the model with 2 strokes for the flow at 20° incidence

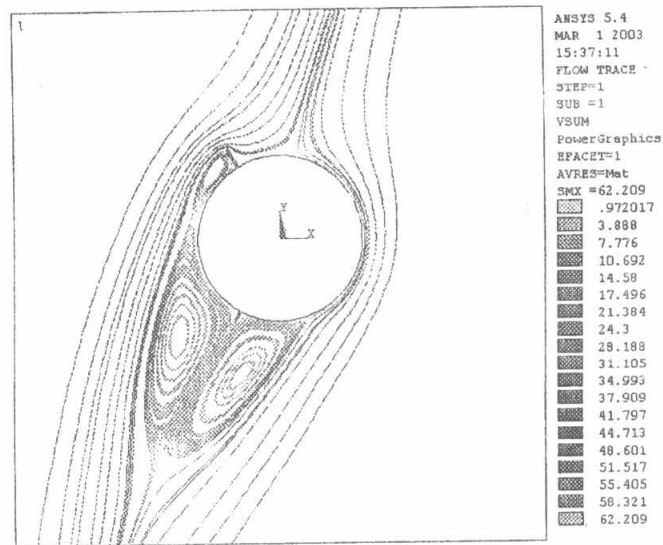


Fig.10 Particles flow traces for the model with 2 strokes for the flow at 20° incidence

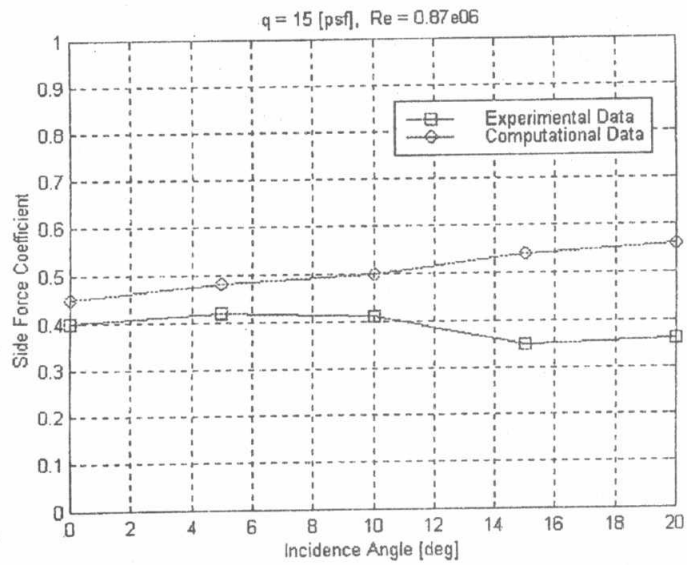


Fig.11 Variation of the side force coefficient with flow incidences of the circular section with strakes for the NASA wind tunnel measurements [2.] and Computational results

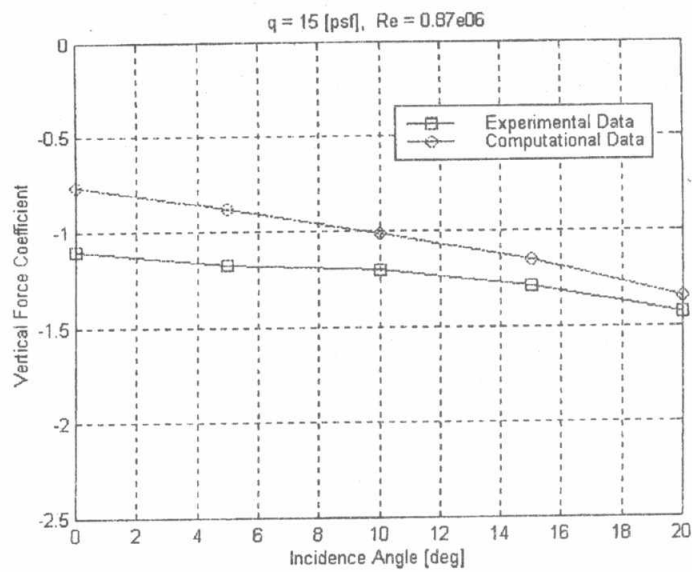


Fig.12 Variation of the vertical force coefficient with flow incidences of the circular section with strakes for the NASA wind tunnel measurements [2.] and Computational results

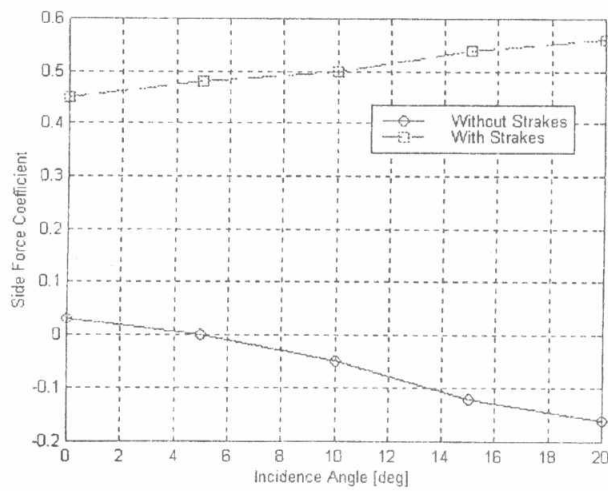


Fig. 13 Comparison of the variation of side force coefficient with flow incidences for the case with/without strakes

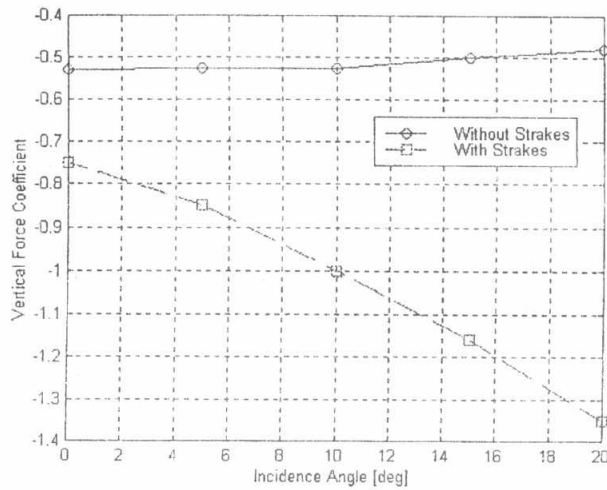


Fig. 14 Comparison of the variation of vertical force coefficient with flow incidences for the case with/without strakes